The International Journal of Advanced Manufacturing Technology (2024) 134:5413–5429
https://doi.org/10.1007/s00170-024-14296-y

ORIGINAL ARTICLE

Single artifact inverse RCSA with improved cross compliance identification

Matej Sulitka[1] · **Jiri Falta**[1] · **Peter Kohut**[1]

Received: 8 April 2024 / Accepted: 14 August 2024 / Published online: 20 September 2024

Abstract
The Frequency Response Function (FRF) at the tool-tip is an important input for machining dynamics prediction, but its measurement is a time-intensive process. The receptance coupling technique offers a faster alternative, suitable for industrial applications where there is experimentally identified receptance matrix at machine-tool holder interface containing enough degrees of freedom to allow connection with various compliant tools modeled using finite element analysis (FEA). The presented approach to the technique further develops simplification of the inverse RCSA by using a single artifact proposed by Montevecchi, presenting a simpler and more general mathematical formulation of the receptance matrix identification. The study also looked into how simplifying tool models affects their accuracy and performance in FEA, aiming to find a good balance between detail and efficiency. To prove the proposed technique, thorough tests on two dynamically different machine tools were conducted with various tool geometries.

Keyword Inverse receptance coupling substructure analysis · Milling · Machine tool dynamics · FRF Identification

1 Introduction

Receptance coupling techniques have been used in machine tool applications for over two decades. These techniques are primarily used to couple machine structures and spindles with various tool types. A significant challenge in machine tool dynamics is determining machining stability to avoid chatter. The stability depends on tool-tip dynamic compliance which varies for each machine-holder-tool pairing and direct experimental evaluation of the dynamic compliance for each assembly would be inefficient. The receptance coupling methods offer a solution how to take into account the change of the tool. As many researchers have contributed to enhancing the applications of receptance coupling techniques, a detailed review is presented in [1] by Schmitz et al.

Receptance coupling methods combine the measured dynamic attributes of the machine structure (without a tool) with the simulated dynamics of different tools. These substructure dynamics are represented by frequency response functions. Determining the dynamics of a composite system when the behavior of its components is known is straightforward. A primary challenge lies in identifying the dynamics at the machine-holder interface, where the holder-tool models are to be connected. This identification must consider not only translational FRFs (position/force) but also rotational FRFs. Multiple methodologies have been proposed by various researchers to address this. Many techniques adopt the approach presented by Schmitz, which infers rotational degrees of freedom at the machine-holder interface using direct frequency response functions measured on short, stiff artifacts [2].

Further, Kim et al. [3] introduced multiple compensation methods to mitigate the uncertainties arising from the previously mentioned approach developed by Schmitz in estimating rotational degrees of freedom (DOFs). For instance, one strategy involves computing the rotation/moment receptances using modal analysis and modal parameters. Other authors have proposed techniques for tool-tip FRF evaluation considering rotating spindle conditions [4–6] where spindle dynamics, measured via non-contact techniques, are combined with simulated tool dynamics.

Kumar et al. [7] measured an artifact–machine assembly and fitted experimental data in the neighborhood of each eigenfrequency using a specific beam characterized by the

✉ Jiri Falta
j.falta@rcmt.cvut.cz

[1] Research Center of Manufacturing Technology (RCMT), Faculty of Mechanical Engineering, Czech Technical University in Prague, Prague, Czech Republic

tuned length and diameter to obtain all machine-end connection FRFs, including rotational DOFs. The synthesis approach, in which rotational DOFs are computed from direct and cross FRFs measured on standard artifacts, is used. Tool-tip FRFs are then calculated using RCSA as a holder, and tool beam models are considered. The coupling is limited to 2D cases and hence many of the cross elements in the receptance matrix are neglected, as similarly in [8], where rotation/moment components of the FRF matrix at the tool adapter free end are found via modal superposition of estimated modal parameters. According to the authors, any tool with the same interface can be coupled with the evaluated interface receptance matrix. The proposed method is compared with the simulated FRF and is experimentally validated for rigid connection.

The rotational degrees of freedom in single-point coupling are not the only way how to model the dynamics of the assembled system. Some authors consider connections at two or more points with translational degrees of freedom instead of a single-point connection incorporating both translational and rotational degrees of freedom. A multi-point modification of RCSA is described by the authors of [9] (Schmitz et al.) where connection between holder and tool portion inserted in the holder is coupled in seven points. Tool-tip FRF is then evaluated via the standard RCSA approach for tool blanks considering various blank diameters and lengths. In [10] (Ambrogio et al.), authors discuss the possibility of substructure decoupling without rotational DOFs. Authors compared using raw measured FRFs and curve-fitted FRFs for decoupling. It was found that increasing number of interface DOFs (overdetermining the problem) may not improve unknown FRF estimation. A considerable effort to increase the effectiveness of the RCSA methods is shown by many other authors, e.g., [11] (Mancisidor 2014) who modifies classical approach [12] by Park et al. (2003) by using an analytical model based on Timoshenko beam theory with fixed boundary approach which allows a decrease in number of calculated modes needed.

A disadvantage of the original methods is the necessity to use multiple artifacts for identifying rotational degrees of freedom FRF at single-point coupling. In [13], Montevecchi et al. proposed and tested the coupling method which identifies a connection between machine and tool using tapping tests at two distinct points, eliminating the need of two artifacts for inverse RCSA. In [14], the authors (Liao et al.) updated the technique separating one of the tapping points from the machine-tool interface. The method is limited to planar translation/rotation solved separately. The validation is done on slender tools only.

Another approach is shown in [15] by Ji et al., where authors introduced two compensation strategies increasing the accuracy of methodology described in [2] (Schmitz et al.) used for evaluation of rotation/moment receptance and full receptance matrix.

Another potential source of uncertainty in the predicted FRF at the tool's tip is the accuracy of finite element analysis (FEA) based models representing the tools. In [16], (Qi et al.) the authors compared Timoshenko and Euler–Bernoulli beam representations of tool body in tool-tip FRF prediction using RCSA and verified the method on simplified slender cylinders representing tool geometries differing in lengths. Albertelli et al. [17] present an improved RCSA method where rotation/moment receptance is estimated via 9 dynamic compliance measurements on spindle-holder assembly and spindle-holder-tool assembly and "new tool" receptances are calculated via 3D FEA.

Gibbons et al. [18] analyzed errors of rotation DOF, synthesis when non-exact measured data are used and proposed optimized measurement spacing using generalized analytical error analysis. On the other hand, some authors, e.g., Gibbons et al. [19] and Kratas et al. [20] focused on tool holder design optimization to enhance chatter stability via modal interaction resulting in dynamic absorber effect. Mohammadi et al. [21] tested a similar approach enhancing chatter stability by tuning tool length or holder and spindle dimensions.

As noted, Park [12] used two artifacts for identification—a very small one, used for obtaining translational FRFs at the interface point, and a longer one used in the aforementioned formulation. Knowledge of translational FRFs simplified the task to such an extent that other FRFs between rotation DOFs and force or torque could be calculated in a form of an analytical formula. Drawbacks of the method include overlooking the influence of the small artifact properties (length, mass, stiffness) on the FRF at the interface point, introducing an error into the method and limitation in the interface point choice.

Munoa et al. [22] provide a critical review of chatter suppression techniques in metal cutting together with the best solution evaluation procedure to deal with chatter problem. The RCSA method is required at tool/tool-holder selection part of the chatter solution problem.

An in-process identification of an FRF of the spindle is proposed in [23] by Postel (2018) which allows to evaluate rotational speed FRF dependency together with feed-dependent spindle shaft FRF. Two methods are compared by the authors, impact tests and inverse stability solution, for spindle FRF evaluation.

Kiran et al. [24] implemented inverse RCSA to eliminate the influence of accelerometer mass loading and cable energy dissipation on FRF measurements. Ozsahin et al. [25] used structural modification method to compensate mass loading effect of accelerometers on tool point FRF measurement improving chatter stability predictions.

Tunc [26] proposed an approach which combines the RCSA method with a STL (stereolithographic) slicing algorithm to enhance the precision of calculating cross-sectional properties of cutting tools. The algorithm exhibits good accuracy in cross-sectional property calculations and is efficient compared to classical FEM calculations. Likewise, Brecher [27] proposed an algorithm to simplify complex tools into beam models, streamlining the computational process.

In this paper, the improvement of inverse RCSA is introduced with a focus on the identification of full receptance matrix with cross compliance elements at the tool-holder interface, using Finite Element Analysis (FEA) for both the artifact and the tool modeling. It also examines the development of simplified models for holder-tool subassemblies and how this simplification influences the accuracy of the tool's Frequency Response Function (FRF). The study further discusses the challenges in RCSA, particularly in creating efficient methods for analyzing machine-holder-tool models and assessing the tool-tip FRF. An experimental procedure for measuring machine FRF is suggested, favoring a single artifact measurement approach over the conventional short and long artifact approach.

The improvement of the RCSA technique, presented in this paper, reduces the necessary data sets for machine dynamics identification via modal excitation response measurements. The employment of a single artifact accelerates the identification process, making it more efficient. To the best knowledge of the authors, a review of existing literature indicates that RCSA methods are commonly applied for systems with minimal impact of cross compliances. In contrast, the presented technique integrates extensive spatial frequency transfer functions, encompassing cross compliances. Another issue addressed by the presented research is a verification of a tool body (holder-tool subassembly) FE model representation by using the Timoshenko beam elements with mass compensation corresponding with the real 3D geometry of tool bodies.

The paper is structured as follows: The next two sections introduce the mathematical formulation of the proposed strategy and cutting tools modelling by Timoshenko beams. Experiments concerning machine tools are detailed in the fourth section. There follows a demonstration of the approach on dynamically different machine tools and tool assemblies. Conclusion and discussion of the results are finally presented to complete the article.

Regarding the nomenclature in this paper, tool is used to denote cutting tool, holder describes tool holder, tool body describes holder-tool subassembly, and artifact is used to denote test tool or blank. Cutting tools used in experiments are referred to as T-XXX-YY where XXX is characteristic tool diameter in millimeters and YY is a number of tool teeth.

2 Updated single artifact inverse RCSA approach

The mathematical formulation of the problem is treated in this section. The idealized planar interface (point) between the machine and the tool (or holder-tool subassembly), where the connection is established, has 5 degrees of freedom (DOFs)—three translational and two rotational, excluding tool rotation around its axis. The primary task is to identify the frequency transfer matrix corresponding to these degrees of freedom. A challenge arises as we only measure force excitation and the acceleration responses. The rotational reaction to force loading, rotational reaction to torque loading, or positional reaction to torque loading must be derived indirectly at the interface point from this data. To account for torque loading or to identify point rotation, we employ an artifact. This tool provides a lever arm allowing for torque application and rotation identification. The dynamic properties inherent to the artifact must be considered and are modeled using the Finite Element Method (FEM).

The approach introduced in this paper builds on a solution developed by Montevecchi [13, 28] and generalized by Liao [14] that involves using a single artifact for identification purposes. The disadvantage of current methods is that the overall compliance matrix is constructed from small elemental matrices representing transfer functions in the plane. When excitation in the X direction is considered at points 1 and 2, the influence of displacement in the X direction and rotation around the Y-axis is considered, and based on this, the receptance matrix (in the plane) is reconstructed. However, this implicitly means that cross-receptances are neglected. For instance, the matrices corresponding to the planar translation and rotation in X–Z and Y–Z plane are as follows:

$$\left[H_{44}\right]_{\mathrm{X-Z}} = \begin{bmatrix} \frac{u_x}{F_x} & \frac{u_x}{M_y} \\ \frac{\varphi_y}{F_x} & \frac{\varphi_y}{M_y} \end{bmatrix} \tag{1}$$

$$\left[H_{44}\right]_{\mathrm{Y-Z}} = \begin{bmatrix} \frac{u_y}{F_y} & \frac{u_y}{M_x} \\ \frac{\varphi_x}{F_y} & \frac{\varphi_x}{M_x} \end{bmatrix} \tag{2}$$

where u_x is the displacement in X direction, φ_y is the small rotation about Y-axis, F_x is the force in X direction, and M_y is the Y component of a torque. A similar notation is used in the case for the Y–Z plane.

The resulting receptance matrix $\left[H_{44}\right]_{\mathrm{2D}}$ composed of the elements of Eqs. (1) and (2) neglects cross-receptances, as shown below by the zero elements.

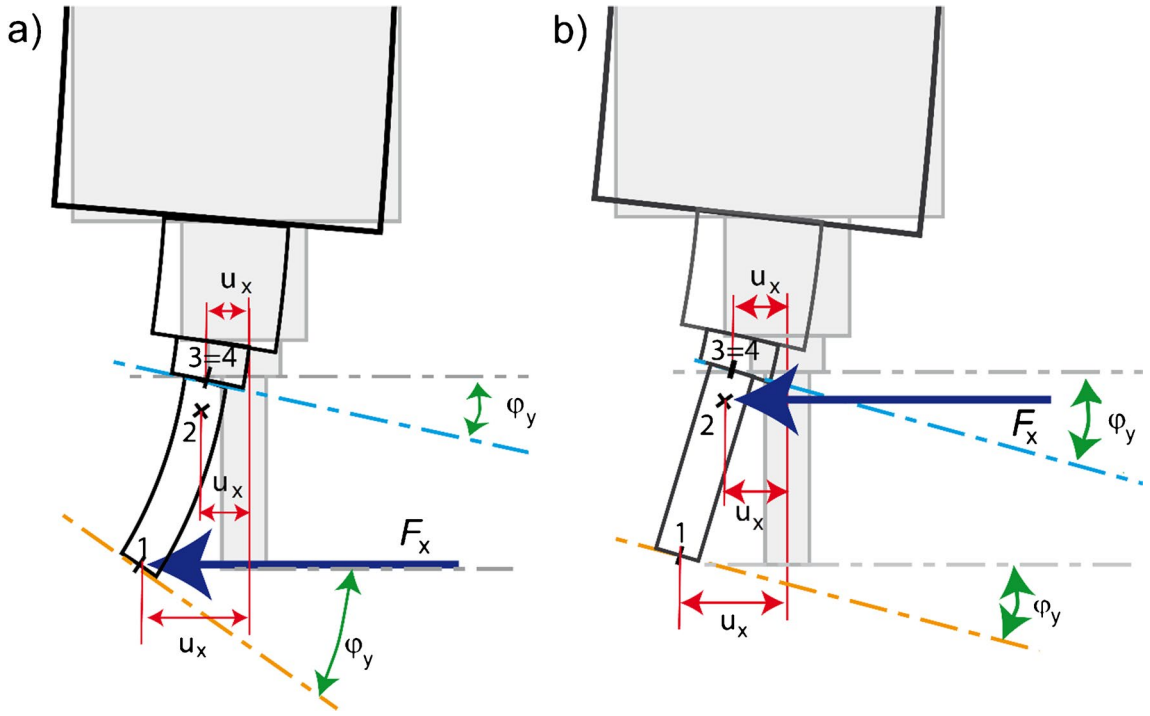

Fig. 1 Schematic view of excitation points during modal impact testing, **a** excitation at point 1 at the free end of the artifact, **b** excitation at point 2 at the fixed end of the artifact. Responses are measured at both points for each excitation. Point 3 represents an idealized artifact–machine interface

$$\left[H_{44}\right]_{2D} = \begin{bmatrix} \frac{u_x}{F_x} & 0 & 0 & 0 & \frac{u_x}{M_y} \\ 0 & \frac{u_y}{F_y} & 0 & \frac{u_y}{M_x} & 0 \\ 0 & 0 & \frac{u_z}{F_z} & 0 & 0 \\ 0 & \frac{\varphi_x}{F_y} & 0 & \frac{\varphi_x}{M_x} & 0 \\ \frac{\varphi_y}{F_x} & 0 & 0 & 0 & \frac{\varphi_y}{M_y} \end{bmatrix} \tag{3}$$

Such a matrix accurately describes the dynamics of the eigenvectors align with the directions of the X, Y, and Z axes. If the eigenvectors do not align with these axes, which they generally do not, non-zero cross-terms will appear. The objective of the proposed method presented in the next section is to identify the full 5×5 receptance matrix, including these cross-terms. An experimental approach is similar to that of Montevecchi—it requires performing impacts and excitations at two specific points and establishing a connection at a third point, which is located near point 2, close to the base of the artifact. The difference is that cross receptances on the assembly need to be measured—either by 3 axial accelerometers or by separate measurements using a 1-axis accelerometer. The approach is schematically shown in Fig. 1. Points 1 and 2 are designated as the impact locations on the artifact, which is held within the machine, while point 3 serves as the interface point. The application of the inverse RCSA method follows these steps:

1. The test artifact is clamped in the machine and subjected to modal hammer impacts at point 1 in the X, Y, and Z directions and at point 2 in the X and Y directions. Responses are recorded at both points, and matrices representing Frequency Response Functions (FRF) are constructed, accounting for both positional and force transfers.
2. A Finite Element Method (FEM) model of the artifact is created. This model uses beam elements with free boundaries and considers eigenvalues and eigenvectors at points 1 and 2. Transfer matrices are developed to connect points 1, 2, and 3, incorporating both positional and flexural degrees of freedom.
3. The dynamic properties of both the artifact and the tool body itself (holder-tool subassembly) are determined using the FEM model. FRFs are obtained at points 1, 2, and 3 on the artifact, as well as at the tool body itself.
4. The machine's properties at the interface point are determined through the developed mathematical formulations. The knowledge of the dynamic properties of the artifact allows the determination of receptance matrix $\left[H_{44}\right]$ at the interface point 4 on the machine.

Knowing the receptance matrix at the interface and FEA model of the tool, the FRF at the tool-tip (point 1) of the

assembly can be determined. The approach to FEA modeling of the tool will be presented in Sect. 3.

The proposed procedure requires a mathematical description of the problem, allowing for the determination of dynamic properties at the interface point based on the measured and simulated data. This approach is outlined below.

As mentioned above, the significant limitation in the experimental identification is that we are directly able to measure only translational deflections through acceleration and force impulses. The missing rotational degrees of freedom (DOFs) and moment loadings must be inferred indirectly, e.g., using an artifact representing a lever. If we were to consider the receptance matrix for this artifact, due to the mentioned measurement limitations, it would be relatively sparse.

The subsequent procedure primarily relies on designing such an indexing scheme that allows for the selection of known, experimentally measured receptance values. These values, in combination with receptances obtained through FEA, enable the formulation of a matrix equation. This equation is instrumental in computing the unknown elements of the receptance matrix at the interface. The challenge lies in effectively integrating experimental data with FEA modelling to calculate the receptances corresponding to rotational DOFs and moment of force loadings.

Let us consider the receptance matrix $[H]$ of the substructures (machine tool, artifact) consisting of 5×5 block receptance matrix $[H_{MN}]$ at the points M and N. The matrices of the artifact are obtained from FEA analysis of the free artifact. According to the receptance coupling method, this system can be described by the matrix

$$[H]=\begin{pmatrix}[H_{44}] & [0] & [0] & [0]\\ [0] & [H_{33}] & [H_{32}] & [H_{31}]\\ [0] & [H_{23}] & [H_{22}] & [H_{21}]\\ [0] & [H_{13}] & [H_{12}] & [H_{11}]\end{pmatrix} \tag{4}$$

and a matrix $[B]$ that gives information about DOF connections

$$[B]=([\,I]\ -[I]\ [0]\ [0]\,) \tag{5}$$

where [I] is the identity matrix of the same size as $[H_{MN}]$. The individual blocks represent the transfer functions corresponding to three translational and two rotational degrees of freedom (rotation about X and Y axes) at the specified points. The DOFs are numbered from 1 to 5. For example $[H_{21,13}]$ denotes X direction response of the free artifact FEA model at point 2 to force impulse in Z direction at point 1.

The receptance matrix for the coupled system, denoted by G, is given [28] by

$$[G]=([H]-[H][B]^T\left([B][H][B]^T\right)^{-1}[B][H]) \tag{6}$$

which is the basis for the RCSA methods. The objective is to determine the receptance matrix of the machine $[H_{44}]$. To achieve this, matrices $[H_{MN}]$ for $M, N=1.3$ from the finite element analysis of the unrestrained artifact and some experimentally identified FRFs from matrix [G] are available (specifically, displacement/force transfers, i.e., FRFs with the last two indices having values 1, 2, 3).

The basis of the approach developed within this research is the division of matrix [H] into an appropriate block structure, both in terms of FRFs between selected points 1, 2, 3, and 4 and the subsequent division of these blocks into smaller blocks corresponding to translational/force degrees of freedom (index 1,2,3) and rotational/torque degrees of freedom (indices 4, 5). As mentioned above, only position/force FRFs, denoted $[G_{MN,i,j}]$ (i, j = 1, 2, 3) can be measured. For those FRFs, the following holds

$$\left[G_{MN,ij}\right]=\left[H_{MN,ij}\right]-\sum_{k=1}^{5}\sum_{l=1}^{5}\left[H_{M3,ik}\right]\left(\left[H_{33}\right]+\left[H_{44}\right]\right)_{kl}^{-1}\left[H_{3N,lj}\right] \tag{7}$$

Each measured receptance represents a row of the system of equations for the unknown elements of the block $\left[H_{44}\right]$, which we aim to solve. The goal of the following procedure is to formulate a problem that can be solved using standard matrix operations. In the first step, we construct a square matrix $\left[\widetilde{G}\right]$ from the receptances that can be directly measured.

$$\left[\widetilde{G}\right]=\left[\widetilde{H}\right]+[P]\left(\left[H_{33}\right]+\left[H_{44}\right]\right)^{-1}[Q] \tag{8}$$

As known inputs for the Frequency Response Function (FRF), accelerations measured by an accelerometer in the X, Y, and Z directions at two points are used, along with excitations in X, Y, and Z at the end of the artifact at point 1, and in X and Y directions at point 2. This results in 6×5 receptances, from which we intend to construct a square 5×5 matrix, meaning that some receptances will be redundant and can be excluded. Given the stiffness of the artifact, it can be anticipated that the responses in the Z direction at points 1 and 2 will not differ significantly, making the corresponding receptances suitable for exclusion from the matrix

$$\left[\widetilde{G}\right]=\begin{bmatrix}G_{11,11} & G_{11,12} & G_{11,13} & G_{12,11} & G_{12,12}\\ G_{11,21} & G_{11,22} & G_{11,23} & G_{12,21} & G_{12,22}\\ G_{11,31} & G_{11,32} & G_{11,33} & G_{12,31} & G_{12,32}\\ G_{21,11} & G_{21,12} & G_{21,13} & G_{22,11} & G_{22,12}\\ G_{21,21} & G_{21,22} & G_{21,23} & G_{22,21} & G_{22,22}\end{bmatrix} \tag{9}$$

Similarly, we will construct corresponding matrices from FEA-based receptances of the artifact

$$\left[\widetilde{H}\right] = \begin{bmatrix} H_{11,11} & H_{11,12} & H_{11,13} & H_{12,11} & H_{12,12} \\ H_{11,21} & H_{11,22} & H_{11,23} & H_{12,21} & H_{12,22} \\ H_{11,31} & H_{11,32} & H_{11,33} & H_{12,31} & H_{12,32} \\ H_{21,11} & H_{21,12} & H_{21,13} & H_{22,11} & H_{22,12} \\ H_{21,21} & H_{21,22} & H_{21,23} & H_{22,21} & H_{22,22} \end{bmatrix},$$

$$[P] = \begin{bmatrix} H_{13,11} & H_{13,12} & H_{13,13} & H_{13,14} & H_{13,15} \\ H_{13,21} & H_{13,22} & H_{13,23} & H_{13,24} & H_{13,25} \\ H_{13,31} & H_{13,32} & H_{13,33} & H_{13,34} & H_{13,35} \\ H_{23,11} & H_{23,12} & H_{23,13} & H_{23,14} & H_{23,15} \\ H_{23,21} & H_{23,22} & H_{23,23} & H_{23,24} & H_{23,25} \end{bmatrix},$$

$$[Q] = \begin{bmatrix} H_{31,11} & H_{31,12} & H_{31,13} & H_{32,11} & H_{32,12} \\ H_{31,21} & H_{31,22} & H_{31,23} & H_{32,21} & H_{32,22} \\ H_{31,31} & H_{31,32} & H_{31,33} & H_{32,31} & H_{32,32} \\ H_{31,41} & H_{31,42} & H_{31,43} & H_{32,41} & H_{32,42} \\ H_{31,51} & H_{31,52} & H_{31,53} & H_{32,51} & H_{32,52} \end{bmatrix}. \quad (10)$$

The unknown matrix block $[H_{44}]$ can be expressed from the relation in Eq. (8).

$$[H_{44}] = [Q]\left(\left[\widetilde{H}\right] - \left[\widetilde{G}\right]\right)^{-1}[P] - [H_{33}] \quad (11)$$

assuming that $[Q]$, $[P]$ and $\left(\left[\widetilde{H}\right] - \left[\widetilde{G}\right]\right)$ are invertible. It should be noted that the receptance matrices are frequency dependent so this must be solved for each frequency separately. This procedure is algorithmically outlined in the Appendix of this article. The obvious advantage of this procedure is that it does not enforce zero cross-receptances, as is the case when the problem is solved using the usual approach in the X–Z and Y–Z planes separately (e.g., recent [1, 29, 30]), see the enforced zero elements of the full receptance matrix in Eq. (3).

The connection of an actual tool can be straightforwardly carried out using Eq. (6). In this case, the matrix $[H_{MN}]$ (M,N < 4) is assembled based on the FEM of the tool being connected. In the comparison presented below, the FEA models of the artifact or the cutting tool were obtained from eigenvector matrices $[V]$ and matrix $[\Omega]$ containing eigenfrequencies on its diagonal. The eigenfrequencies and eigenvectors are obtained from Ansys WB. The advantage of using Timoshenko beam finite elements is that they have both translational and rotational degrees of freedom at each node. In the case of using a volumetric mesh and linear elements, it is necessary to calculate the rotational degrees of freedom from the displacement values at several nodes or use tools such as a *remote point* in Ansys WB. The matrix of eigenvectors was constructed such that it contains the eigenvectors normalized to modal mass in columns, each vector consisting of five elements corresponding to translational and rotational degrees of freedom for each nodal value at the interface or tapping points 1,2,3. The eigenvector corresponding to the i-th eigenfrequency Ω_i is than

$$V_i = \left(V_{1,ix}, V_{1,iy}, V_{1,iz}, V_{1,i\varphi_x}, V_{1,i\varphi_y}, V_{2,ix}, \ldots, V_{3,i\varphi_y}\right)^T \quad (12)$$

In this case, the translational degrees of freedom were denoted x, y, z and rotational φ_x and φ_y instead of numbers for better readability. The frequency-dependent receptance matrix $[H]$ of the artifact or tool can be expressed as follows:

$$[H](\omega) = [V]\left([I]\omega^2 + 2\zeta\omega[\Omega] + [\Omega]^2\right)[V]^T, \quad (13)$$

where ω is the angular frequency of the excitation, and ζ is the proportional damping which is typically set to zero. The implementation of inverse RCSA and the assembly of transfer matrices based on eigenvectors and frequencies from FEA is provided in the sample script attached in the Appendix.

In the next part, the study focuses on challenges associated with tool body modelling using the finite element analysis. It also addresses uncertainties related to the design of the artifact's geometry. The methodology is exemplified through experimentation on two machines with distinct dynamic characteristics and with tools of varying weight and dimensions.

3 Tool body representation by FEA

The main purpose of the RCSA method in machine tool applications is typically to evaluate tool-tip FRF of the machine-spindle-holder-tool assembly as was mentioned earlier. In such case, an FRF of machine part of the assembly (including the spindle) is measured experimentally and combined via RCSA method with FRF of the holder-tool part (tool body) of the assembly, which is evaluated using computational techniques.

For applications involving machine tools utilizing the RCSA method, where the primary objective is to assess the dynamic behavior of the machine-holder-tool system at the tool-tip, there is a need to model the holder-tool part (tool body) of the machine-holder-tool system using Finite Element Analysis (FEA).

An approach for modeling tool bodies using Timoshenko beam FE models was applied, tested, and verified, since one of the goals of the presented research is to correctly capture the effects of real 3D tool body geometry.

In Fig. 2 schematic view of the machine-holder-tool assembly can be seen. The *machine* subassembly consists of a machine tool including spindle and a tool holder interface (here the ISO cone). The *tool body* subassembly consists of tool holder (holder) and tool itself.

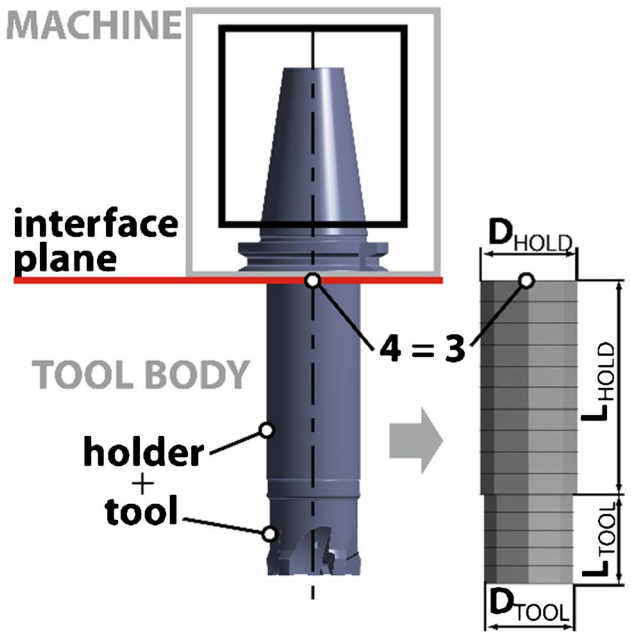

Fig. 2 Schematic view of a machine-holder-tool assembly with interface plane and interface point 4 used for coupling the FE beam representation of tool body (holder-tool subassembly)

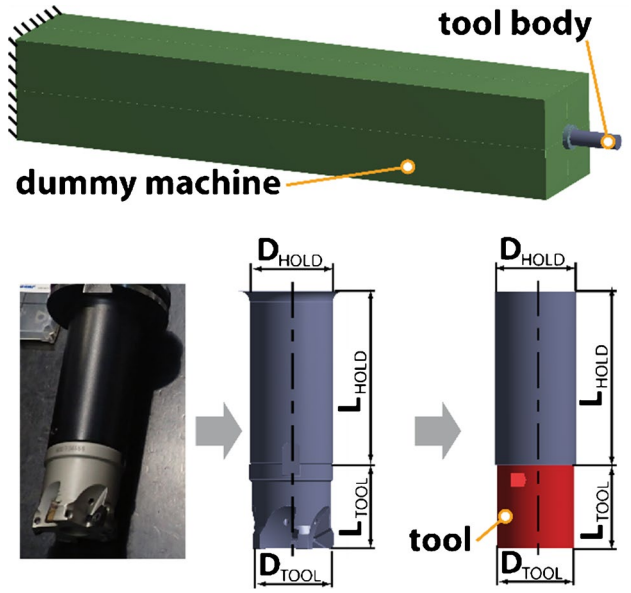

Fig. 3 Square prism dummy machine with tool body geometry connected at interface plane (top) and tool body T-040–05 with holder as a real 3D geometry model with main dimensions and its two-beam 1D representation with red highlighted tool part, density of which is changed (bottom)

Let us consider *tool body* part (Fig. 2) of the whole assembly and let this part to be coupled to the *machine* at interface point 4. In the proposed procedure, the interface point 4 is chosen in a way that the real tool holder interface between *machine* and *tool holder* together with tool holder v-flange is included in *machine* part of the assembly as can be seen in Fig. 2. Thus, only *tool body* part (holder-tool subassembly in Fig. 2) is modeled by FEA.

In proposed approach, a complex real geometry of *tool body* assembly is represented by a set of beams; the size of which (diameter, length) is defined by main dimensions of *tool body* geometry. In practice, the *tool body* geometry can be divided into arbitrary number of sections, depending on the complexity of a real geometry. However, such simplification of the real complex geometry with cavities and grooves leads inevitably to differences in mass and stiffness distribution when real and beam *tool body* geometry is compared.

Different ways to capturing the real *tool body* geometry using the 1D beam elements were investigated including the influence of model parameters. Among the model parameters were the following:

- Dimensions (lengths/diameters)
- Mass/density
- Young modulus
- FRF evaluation point position
- Transition radius between holder and interface plane.

In the following section, we will address the model uncertainty associated with simplifying a tool body 3D model to a 1D beam replacement.

The goal is to provide strategy to model holder-tool assembly (tool body) as 1D beam replacement with density of the tool part changed to reach real tool mass.

In this test the tool body geometry is connected to a simplified dummy machine represented via square prism geometry (Fig. 3) in both cases of detailed and simplified tool body geometry (Fig. 4). The 1st eigenfrequency and static stiffness of the dummy machine geometry are tuned according to a typical machine tool values. The left face of the dummy machine is fixed.

Figure 3 also shows the real tool geometry with nominal diameter of 40 mm and 5 teeth (T-040–05) with holder together with considered main dimensions and resulting 1D representation of the tool body with highlighted tool part, density of which is changed to meet real tool weight

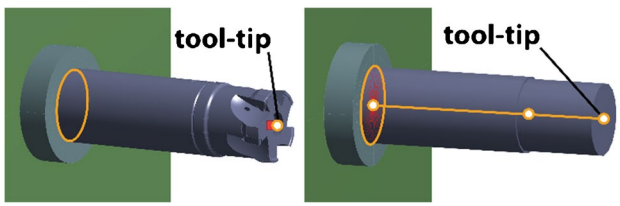

Fig. 4 3D tool body with highlighted contact area between holder and dummy machine at interface plane and tool-tip point (left) together with two-beam 1D tool body representation (right)

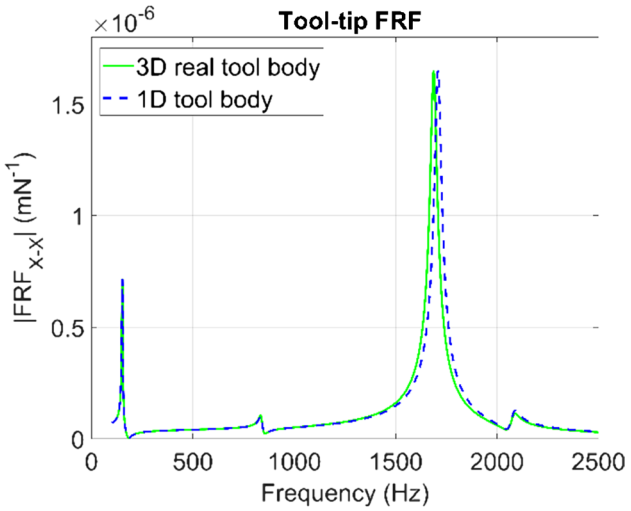

Fig. 5 FEA calculated FRF at tool-tip of dummy machine-holder-tool assembly showing the influence of 3D detailed and 1D beam holder-tool geometry (T-040–05, i.e., 40 mm diameter and 5 teeth)

provided by tool manufacturer. Contact area used for connection to the 1D FE tool model at interface plane corresponds to the tool holder diameter.

The real tool geometry has quite big cavities and thus cylindrical simplification may lead to significant difference in part weight. Therefore, density of the part representing geometry of the tool shall be changed to represent real weight and consequently real dynamic behavior of the holder-tool assembly in form of FRFs.

Figure 4 shows the interface between dummy machine and tool body and tool-tip position for both cases. 3D tool body is connected to dummy machine at contact interface plane, where transition radius between holder and interface plane is neglected (Fig. 4 left). 1D tool body representation and dummy machine are connected via remote points with 1st defined at left end vertex of the tool body and 2nd one on dummy machine face representing holder contact face (highlighted) with transition radius between holder and interface plane neglected (Fig. 4 right), thus the diameters of the contact face on dummy machine are the same for both cases.

An example of a tool-tip FRF comparison between real geometry milling tool body (T-040–05 with holder) and its prismatic representation connected to the dummy machine (Fig. 3) is shown in Fig. 5. Good agreement between tool-tip FRF of 3D detailed and 1D beam model can be observed. Peak frequency shift of less than 25 Hz or less than 2% is observed between 3 and 1D holder-tool representation.

Tests have shown that for achieving good eigenfrequency match on dominant modes, it is especially important to ensure a comparable distribution of mass in the beam cylindrical substitutes as in the actual tool system. The distribution of mass is significantly influenced by cavities and volume recesses on the tool. Given that the diameter of the beam substitute is derived from the tool diameter, the comparable mass distribution is achieved by adjusting the density of the cylindrical beam part corresponding to the tool.

Another possible approach is modification through the tool diameter of a lumped tool. This is more physically appropriate if the grooves or cavities on the tool are close to the perimeter (because of better approximating the second moment of area), as it also better models the change in tool stiffness. On the other hand, modification by density is more suitable for cavities near the tool axis. In the case of the studied robust tools, the approaches were comparable, and from a practical standpoint, we found the density modification for the studied tools more practical. The reason is that it was simpler to weigh the tools when creating the database and transform the lumped tool density accordingly. However, this approach might not be suitable for slender tools. For such tools, it would be better to either use the diameter modification or to model the beam elements based on real cross sections [26].

4 Experimental testing

The measurements were carried out on the vertical machining center MCVF 1260i produced by TAJMAC-ZPS and the horizontal machining center WHT 110 produced by TOS VARNSDORF A.S (Fig. 6). These machines were selected due to their different design concepts, dimensions, and dynamic properties. MCVF1260i is a small-size three-axes center with the travel lengths of 1300 mm along the X-axis, 640 mm along the Y-axis (both axes on the table), and 800 mm along the vertical Z-axis. The tested machine utilizes an ISO 40 type tool holder interface. Contrary to this, WHT 110 is a mid-size horizontal boring and machining center with the travel length along the X-axis 3000 mm, Y-axis 2000 mm, and Z-axis 2500 mm. The machine is equipped with ISO 50 type tool holder interface.

In the case of the MCFV1260i machine, the dynamic properties of the assembly at the tool-tip change only with its movement in the Z-axis, and even this influence is relatively small. In contrast, the WHT 110 machine exhibits significantly variable dynamics within its workspace, and its properties have therefore been identified at a 4×4 point grid. The dominant influence is exerted by the retractable spindle of the machining machine – the W-axis.

For measurements, equipment consisting of a DAQ card NI 9231, one Brüel&Kjaer modal hammer 8206–003, one Brüel&Kjaer 4524 B1 three-axis accelerometer, and a single-axis accelerometer PCB 352A21 was used.

To identify both translational-force FRF and bending-moment FRF, artifacts measuring $45 \times 45 \times 200$ mm with ISO 50 on WHT110 and $32 \times 32 \times 100$ mm with ISO 40 on MCFV1260i were used (Fig. 7).

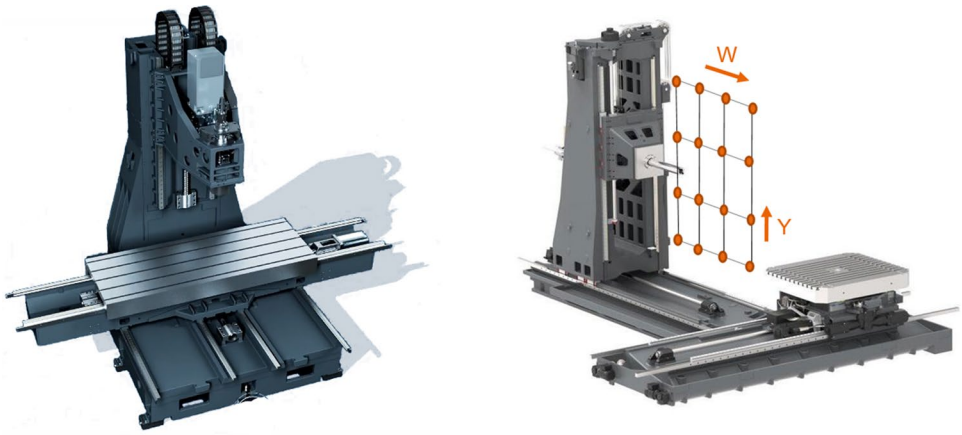

Fig. 6 Machine tools, MCFV 1260i and WHT110, are used for validation. Due to the significantly varying dynamics of the latter machine tool it is identified on a grid of Y and W positions

Fig. 7 Artifacts 45 × 45 × 200 mm for WHT 110 (left) and 32 × 32 × 100 mm for MCFV1260i (right)

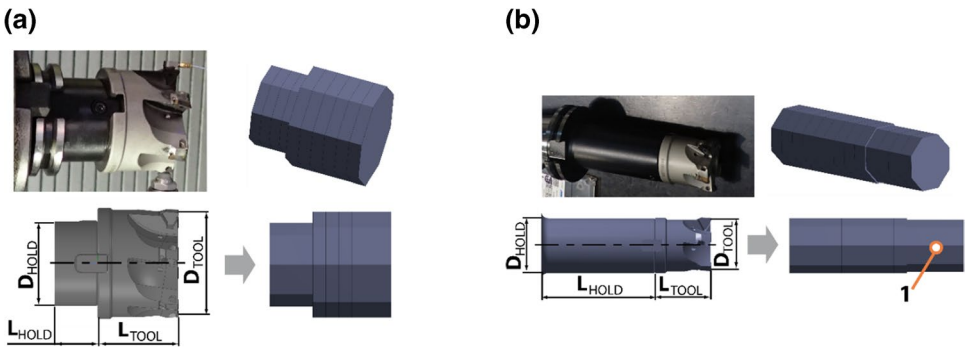

Fig. 8 Comparative visualization of various milling cutters mounted on MCFV1260i alongside their respective beam replacements, illustrating the distinction between the holder-tool part and clamping components and showcasing the specific features of each model. **a** Milling cutter T-063–06. **b** Milling cutter T-040–05

In order to experimentally test the robustness of the approach, two milling tools denoted internally as T-063–06, T-040–05 were selected for *MCFV1260i* and two milling tool denoted T-063–04 and T-160–09 were selected for WHT 110. These tools have been chosen specifically because they are robust, making their 1D beam representation more straightforward. Slender monolithic tools were so far excluded from comparison due to the challenges they pose for 1D beam representation which are covered in other articles.

Let us briefly introduce the *MCFV1260i* milling tools used for validation, see Fig. 8. For T-063–06, the 1D representation is composed of two beams. The shorter one captures the holder section between the tool and the defined interface plane that separates the system into machine and holder-tool components. The longer beam represents the actual tool. Notably, the density of this tool is adjusted to account for its weight and cutouts.

Tool T-040–05 also employs a beam-based 1D representation, which again omits the clamping interface. The longer of the two beams models the holder section from the interface plane to the tool, while the shorter beam stands for the tool itself. It's important to mention that the density remains constant and that there is a suggestion to adjust the position of a reference point closer to the actual point of deflection.

Figure 9 shows the tools selected for WHT 110 validation. For T-063–04, the longer beam represents the holder section between the interface plane and the tool, while the shorter one represents the tool itself. The density of the tool is adjusted in this case as well to maintain its mass while the geometric dimensions remain unchanged.

Lastly, T-160–09 has a 1D model comprising four beams, two for the holder section and two for the tool section. One of these beams is a hollow cylinder to account for a specific mass distribution at the free end of the tool. This beam's density is subsequently modified to reflect its actual volume.

In summary, each holder-tool's 1D representation effectively maintains essential parameters such as density and dimensions, allowing for computational analysis while bypassing the complexities associated with their geometries.

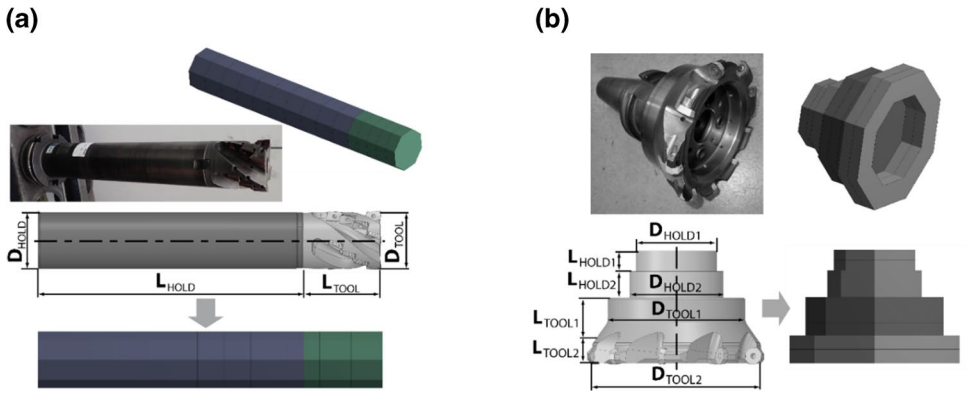

Fig. 9 Comparative visualization of various milling cutters mounted on WHT110 alongside their respective beam replacements, illustrating the distinction between the holder-tool part and clamping components and showcasing the specific features of each model. **a** Milling cutter T-063–04. **b** Milling cutter T-160–09

One of the important issues is the selection of the artifact dimensions. The ideal artifact would be an absolutely rigid, long, and weightless lever. However, in reality, these requirements conflict with each other. It is necessary to make a trade-off between the length and cross-section of the artifact. For this purpose, a test was conducted on two artifact geometries—a larger one with dimensions of 45×45×250 mm and a smaller one of 32×32×100 mm. A series of tests on a dynamically comparable machine to MCFV1260i showed that the smaller artifact provided more reliable results for the chosen tool bodies. The stiffness of the smaller artifact is approximately 4 times higher than the longer one and also it has 5 times lower weight. One of the tests was a cross-test between these artifacts.

In the first test, the larger artifact was used for the identification of the FRF from the interface, and validation was done on the smaller artifact, and vice versa. The results can be seen in Fig. 10. This result provided only an approximate guideline for selecting the dimensions of the artifact. For the more robust WHT 110 machine with an ISO50 holder, the size of artifact 45×45×200 was chosen without further testing. The motivation for a longer length at the expense of the stiffness and a higher weight, was to capture the effect of rotational degrees of freedom at greater extension of the spindle. A larger cross-section of the artifact would then be impractical due to high weight and the availability of a semi-finished product for such an artifact.

5 Experimental validation of the modified RCSA technique

For the verification of the method and its sensitivity to the identification of machine characteristics and the accuracy of FEA modeling, tests were conducted on the machines and tool bodies described in the previous chapter. The analysis is done on a case-by-case basis.

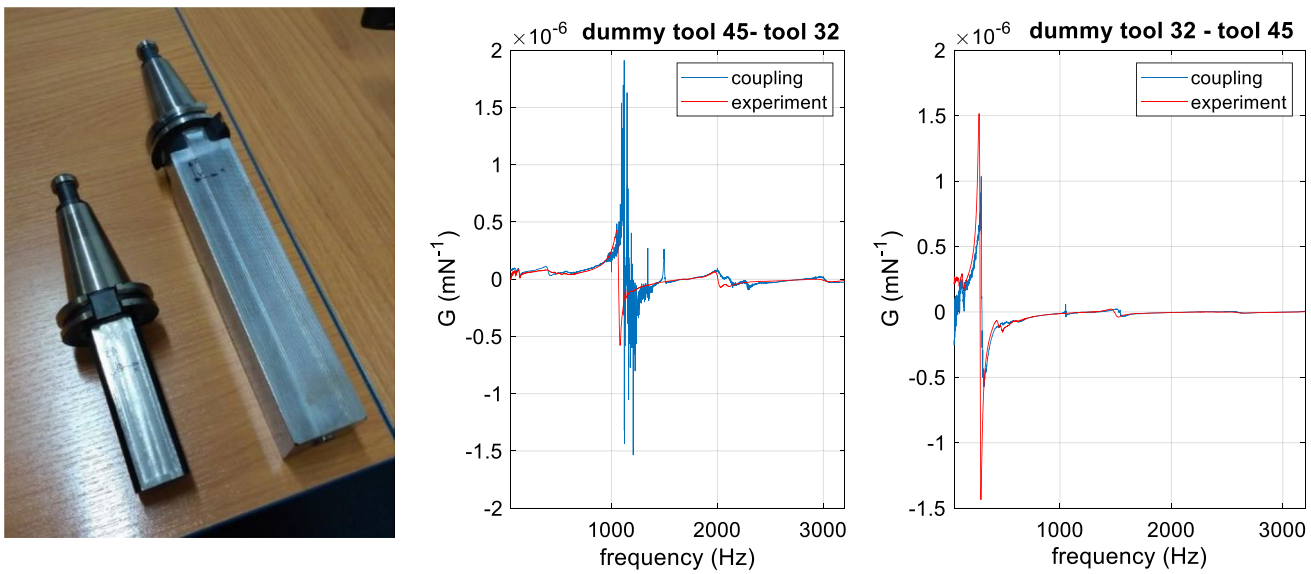

Fig. 10 Cross-validation of the artifact geometry. In the photograph, on the left, there is an artifact with dimensions of 32×32×100 mm, and on the right, one with dimensions of 45×45×250 mm

The following tests were conducted on a three-axis milling machine, the MCFV1260, which was equipped with two tool bodies: the compact T-063–06 and the slender T-040–05. The results of the experimental validation are given in Fig. 11. Comparison between the predicted and directly measured Frequency Response Function (FRF) at the tool-tip shows a good match. The exception to this is the FRF in the X direction for T-063–06 tool body, where the observed deviation was noteworthy. In this instance, while the frequency of the dominant mode was accurately predicted, there was a significant discrepancy in the amplitude. The discrepancy might be due to matrix inversion in Eq. (11), although the condition number is not significantly worse in the area. The issue of how to increase the method's robustness is the subject of further research.

The experiments conducted on the WHT 110 C milling machine, equipped with an extendable spindle, have shown that the W-axis positioning significantly affects the machine's dynamic behavior. The experimental results have been comparatively demonstrated on two distinct tools bodies: the compact T-160–09 and the slenderer T-063–04. Due to the significant differences in dynamics with respect to the positions on the Y and W axes, the FRF on the tool bodies is analyzed in more detail. For the tool body T-160–09, a comparison is conducted at two points in working space, A and B, as indicated in the scheme in Fig. 12.

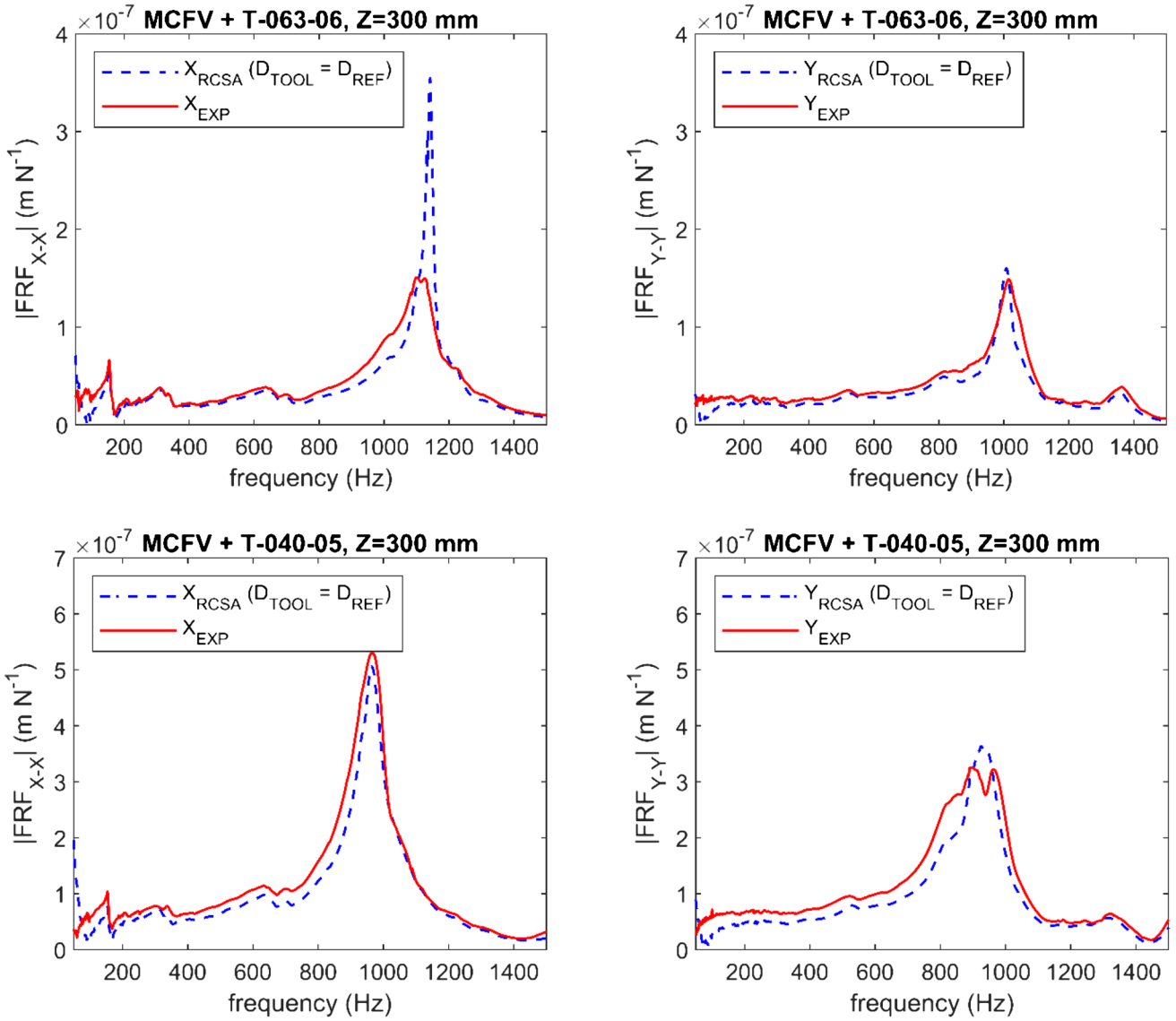

Fig. 11 FRF validation for the robust T-063–06 and slender T-040–05 on MCFV1260. The left graph shows direct FRF in X direction, right on in Y direction

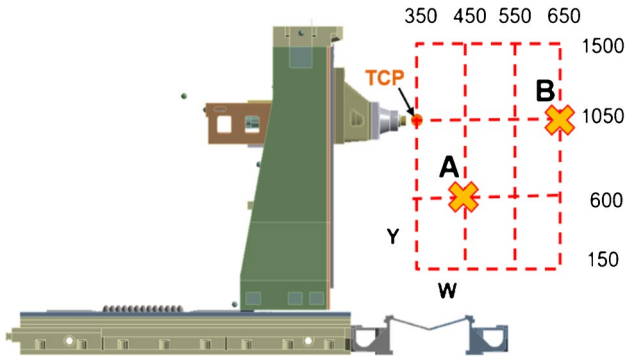

Fig. 12 Scheme of the measured positions in Y and W axes

The graphs in Figs. 13 and 14 show a good match of the experimentally identified FRF and the RCSA-predicted FRFs at the tool-tip in both X and Y directions. The graphs indicate a significant decrease in the dominant natural frequency at point B as compared to point A. This shift is consistent with a greater extension of the spindle at point B, which typically results in a lower stiffness and consequently a lower natural frequency. The model exhibits a slightly better match for the more compliant (and dynamically simpler) case.

Very good agreement between predicted and experimentally identified FRF is achieved both for the configuration with high compliance on the machine side at maximum spindle extension, where cross-receptances do not play a significant role due to the dominant influence of a dynamically simple

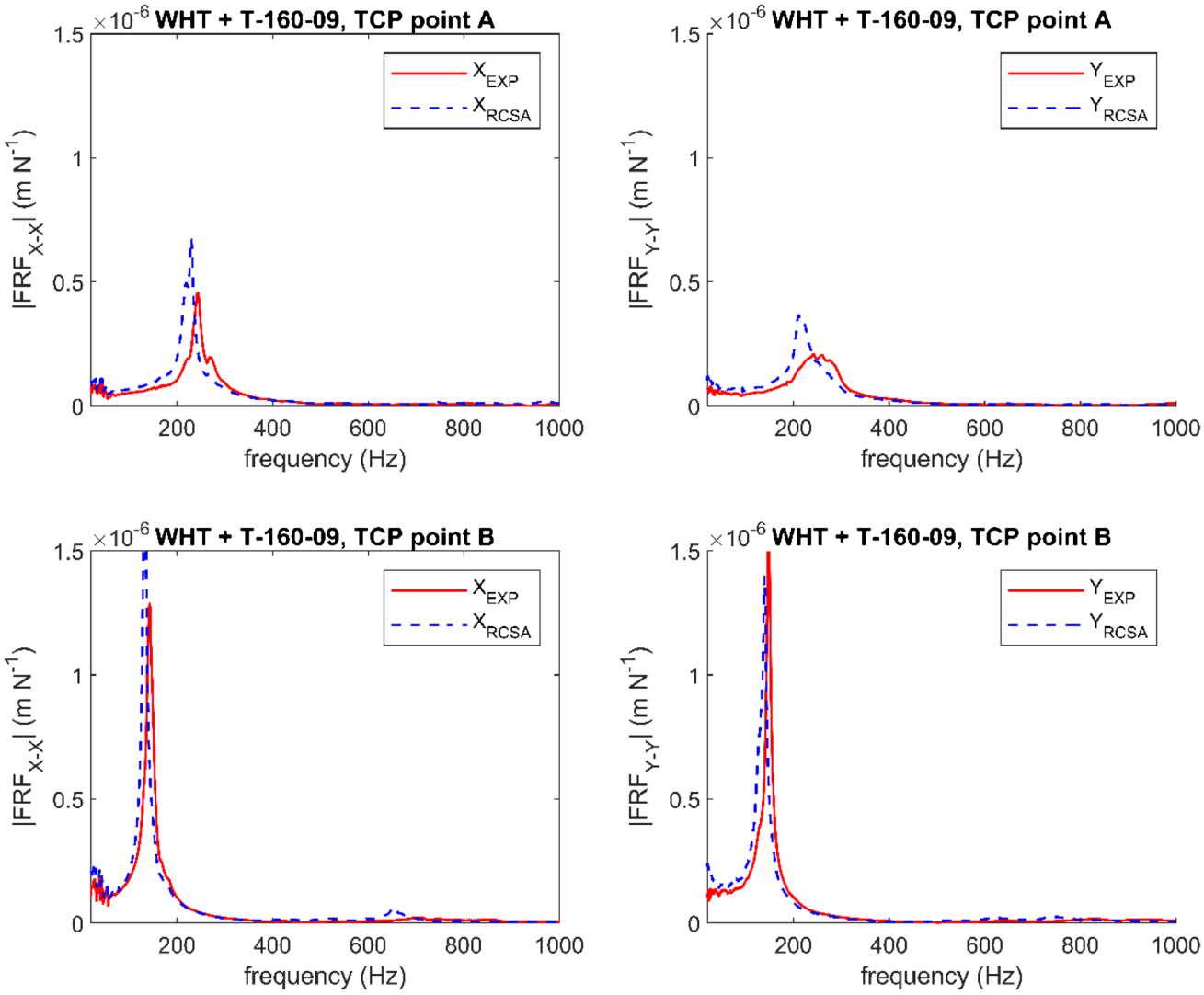

Fig. 13 Results for T-160–09 at positions A and B. The method captures well the frequency change but the amplitudes differ by ca 30% at A and 15% at the point B

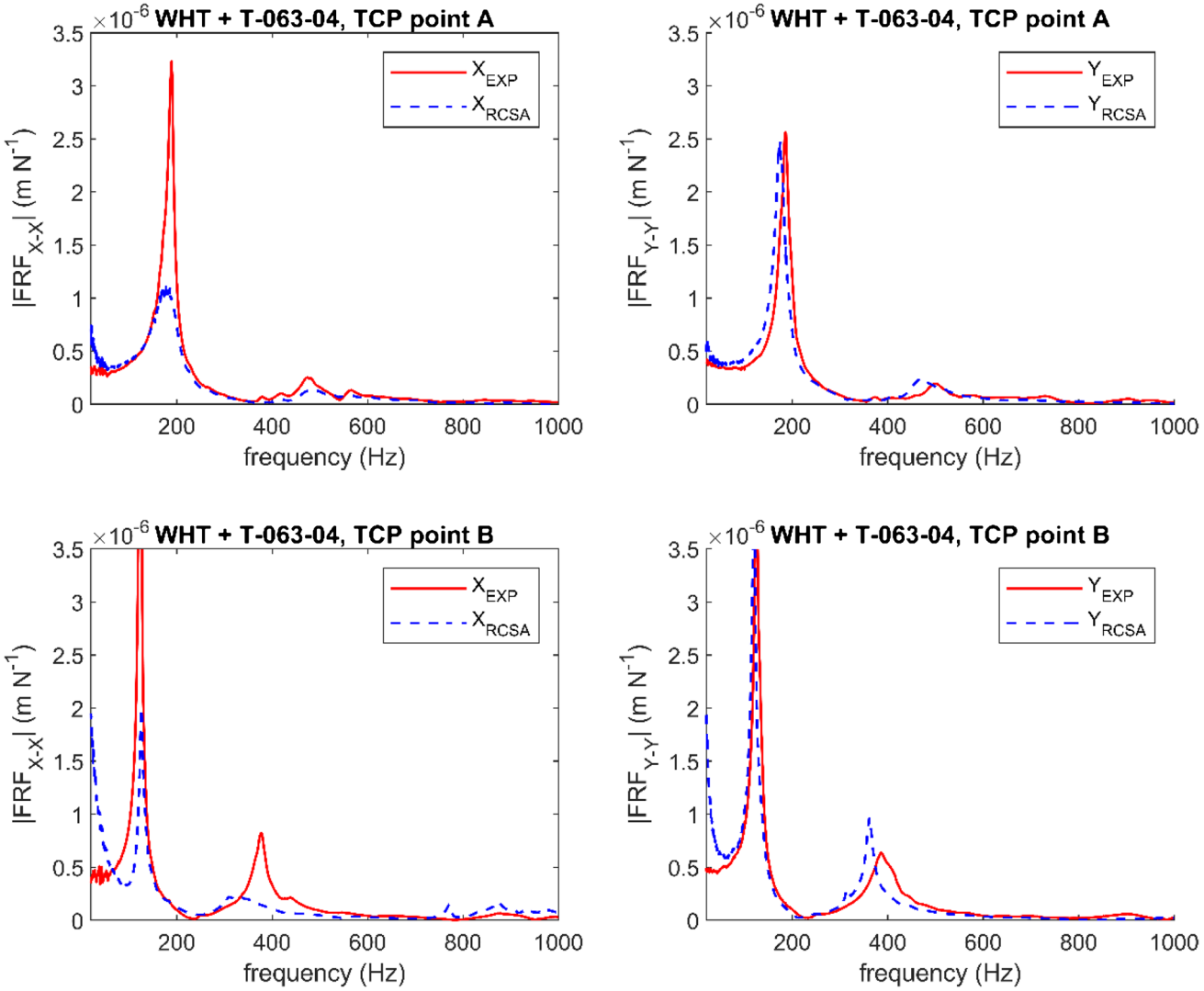

Fig. 14 Results for T-63–04 at positions A and B. The method captures well the frequency change but the amplitudes differ significantly at both points in X-X receptance

spindle, and for the case of lower compliance with the spindle retracted. In this configuration, and similarly. on the more compact machine MCFV1260i, the influence of various modes of the structure can be expected, which may not necessarily correspond to the machine axes. This mentioned agreement confirms the suitability of including all cross-receptances in the receptance matrix at the machine-tool interface.

For both machines and tools, very good match of FRF eigenfrequencies was achieved at dominant modes. In both cases, significant amplitude differences in the direction of one of the machine axes were observed for some combinations of machine and tool. This error occurred on the smaller and stiffer MCFV with a shorter tool, while on the WHT machine with an extended spindle and increased compliance, it occurred with a longer tool. It should be noted that, in contrast to Montevecchi's [13] and Liao's [14] tests, the presented measurements are conducted on more robust machines with massive tools, where the quality of the receptance matrix in the interface is significantly more pronounced than with a slender tool. This is also reflected in the choice of the size of the artifact, which in our case is substantially larger.

We plan to test in further research the relationship of the conditionality of the RCSA problem (both inverse and direct) in connection to the properties of the tool and the spindle.

One of the parameters that seemed to influence the agreement of the prediction with experimental data was the accelerometer used. On the same machine, better agreement seemed to be achieved when using a 1-axis accelerometer compared to a 3-axis one. The significant difference of the accelerometer was their higher frequency range and higher sensitivity—10 kHz frequency range and 1 mV/(m.s^{-2})

for the 1-axis compared to 3 kHz frequency range and 10 mV/(m.s^{-2}) sensitivity for the three-axis accelerometer. However, there is a natural disadvantage of time-consuming measurement with a single-axis accelerometer.

6 Conclusions

The Receptance Coupling Substructure Analysis is an effective method for the prediction of dynamic behavior in coupled machine-holder-tool systems. This paper presents a refined mathematical approach to inverse RCSA, enabling the identification of both translational and rotational elements in the receptance matrix at the single-point machine-holder interface.

The method introduced in this paper advances the strategy of using a single artifact by properly selecting points for tapping with a modal hammer and positioning the accelerometer to obtain reliable cross receptances at the machine-tool interface. This innovative approach overcomes the limitations of 2D simplifications of the translational and rotational FRF in the X, Y, and Z directions, allowing for the identification of more complex cross compliance terms in the matrix.

The primary advantage of this method is that it does not require simplification to a planar case, thereby providing a more accurate compliance matrix at the idealized interface, including all cross receptances. This results in more accurate receptance calculation via inverse RCSA, particularly for machines with complex dynamic behavior where cross receptances are more pronounced. This proposed inverse RCSA calculation is general and can replace traditional methods that use reductions to planar translation and rotation. The calculation procedure is demonstrated in the Appendix. If the cross-receptances are not measured, they can be replaced with zero, and the result will then correspond to the traditional method.

Additionally, a study on testing artifact dimensions is presented. A convenient artifact is characterized by its rigidity, length, and low mass—attributes that are typically in opposition. Research showed that the choice of artifact dimensions can significantly affect the quality of the resulting FRFs.

The validation was done on two structurally and dynamically distinct machine tools, each paired with geometrically varied tools. Compact roughing tools and slender semifinish tools with increased compliancy were tested. Through this research, several critical aspects were explored. The sensitivity of the cutting tool model simplifications through the Finite Element Analysis was studied. A strategy based on 1D beam elements is developed, where the modeling approach uses mass-tuned beam model. This approach proved to provide reliable results in calculating the FRFs at tool-tip by RCSA method. It should be noted that the used FE models both of the test artifact as well as the 1D beam-cutting tool model is undamped. Although this may not universally apply and has been tested on the presented group of tools, the observed good agreement of undamped models is significant from a practical standpoint, as it reduces the complexity of the tool models and the need for their tuning. Originally, considering the presence of joints in the tested tool assemblies, it was assumed that tuning for damping would be required.

The results of the FRF validation using the modified RCSA showed that good agreement is achieved in all machine–cutting tool combinations investigated. For compact tools, which are primarily characterized by mass, the achieved agreement indicates the accuracy of the calculated cross-receptances in the full 5×5 receptance matrix at the machine-tool interface. In the case of longer tools with increased compliance, the agreement achieved also shows the validity of the model representation of the tool using 1D beam FE elements.

Although the described inverse RCSA method with a single artifact is general, the procedure for creating tool replacements has been validated on a specific category of tools. The density modification approach used in this procedure would be more suitable for tools with central cavities as it in that case better approximates the second moment of area in FEA-based beam models. There is an alternative approach using effective tool diameter that would be more effective for tools with peripheral grooves, as it better approximates the second moment of area, thus better modelling changes in stiffness. While both methods were comparably effective for robust tools, density modification proved to be more practical due to its simplicity in data collection and adjustments in tool density. However, for slender tools, modifying the diameter or modeling FEA based on real cross-sections might be more appropriate. (e.g., [26]).

Further research will focus on validating the developed strategy for other combinations of machines and tools and testing the appropriate size of test artifact to minimize uncertainties in the determination of cross compliances in the interface compliance matrix.

Appendix

Determining the receptance matrix using the inverse RCSA method in Matlab

The script below is an algorithmization of the mathematical procedure described in Sect. 2.1. The inputs are FRF measurements on the artifact and FEA models of the artifact and tool. In the first step, transfer functions for the considered undamped tool and artifact will be assembled from the eigenvalue vector and the matrix composed of eigenmodes in the columns as in Eq. (9). These transfer functions are stored in block matrices $[H_{IJ}]$ based on the formula Eq. (10).

```
%% input:
%   EigFrq_art ... vector of artifact eigenfrequencies form FEA software
%   V_art... matrix of artifact eigenvectors form FEA software
%                       see Eq.11
%   EigFrq_tool ... vector of tool eigenfrequencies form FEA software
%   V_tool... matrix of tool eigenvectors form FEA software
%                       see Eq.11
%   FRFm{I,J,k,l}... cell structure for storing measured FRFs values
%         I...accelerometer position (end-1 or root-2 of the tool/artifact)
%         J...force impulse position
%         k... acceleration DOFs: 1=X, 2=Y,3=Z,4=rotX,5=rotY
%         l... force impulse DOFs: 1=FX, 2=FY,3=FZ,4=TorqX,5=TorqY
%            FRF measurement can contain only displacement/force/ responses, not
%            rotation/torque/
%   frqM... vector of FRFs frequencies from measurement
%   G{I,J,k,l}...cell structure for storing calculated FRFs on the tool
%   H_art{I,J,k,l}...cell structure for storing calculated FRFs on the
%   artifact substructure model
%   H_tool{I,J,k,l}...cell structure for storing calculated FRFs on the
%   tool substructure model

dmp=0 %   tool/artifact damping setting

%% cell alocation
H_art=cell(3,3,5,5); %FEA based FRF of artifact
H_tool=cell(2,2,5,5); %FEA based FRF of real tool
G=cell(2,2,3,3);%FEA based FRF of real tool

%% read calculated FEA based FRF of a test tool into the indexed structure H_IJkl
for frq_idx=2:size(frqM,1)
    % Transfer function matrices calculation of test and real tool
    % from eigenvectors and eigenfrequencies based on Eq.12
          TF_art= V_art*...
        (...
           (...
            -(2*pi*frqM(frq_idx)).^2*eye(size(EigFrq_art,1))+...
            2*1i*dmp*2*pi*diag(EigFrq_art)*(2*pi*frqM(frq_idx))+...
            diag(2*pi*EigFrq_art).^2 ...
           )\V_art.'...
        );
    TF_tool= V_tool *...
        (...
            (...
              -(2*pi*frqM(frq_idx)).^2*eye(size(EigFrq_tool,1))+...
              2*1i*dmp*2*pi*diag(EigFrq_tool)*(2*pi*frqM(frq_idx))+...
              diag(2*pi*EigFrq_tool).^2... ...
            )\V_tool.' ...
        );

    for I=1:3
        for J=1:3
            for k0=1:5
                 for l_0=1:5
                    H_art{I,J,k0,l_0}(frq_idx,1)=TF_art((k0-1)*3+I,(l_0-1)*3 + J);
                    H_tool{I,J,k0,l_0}(frq_idx,1)=TF_tool((k0-1)*3+I,(l_0-1)*3 + J);
                 end
            end
        end
    end
end
```

In the next step, the FEA model of the artifact will be subtracted from the transfer functions measured on the clamped shank using the inverse RCSA approach presented in the article. This in the first step means selecting the indices of the FRF measurements used for identifying the translational and bending receptances at the idealized interface between the machine and the tool. The calculation of the receptance is based on Eqs. (9) and (10).

```
%FRF points and directions chosen for 5x5 experimantal FRFs G matrix
%   /for construction of matrices in Eq. 8 and Eq. 9
idx1=[1,1,1,2,2];
idx2=[1,2,3,1,2];
%% subtracting artifact from the assembly + add real tool
for frq_idx=2:size(frqM,1)
% read calculated FEA based FRF of a real tool into the indexed IJkl structure
    %subtract artifact from machine-artifact assembly. the notation
    %corresponds to Eq.10
    for alef=1:5
        for bet=1:5
            I=idx1(alef);
            J=idx1(bet);
            k=idx2(alef);
            l=idx2(bet);

            G_Tilde(alef,bet)=FRFm{I,J,k,l}(frq_idx);
            H_Tilde(alef,bet)=H_art{I,J,k,l}(frq_idx);
            P(alef,bet)=H_art{I,3,k,bet}(frq_idx);
            Q(alef,bet)=H_art{3,J,alef,l}(frq_idx);

            H33(alef,bet)=H_art{3,3,alef,bet}(frq_idx);
        end
    end
    H44{frq_idx}=Q*((H_Tilde-G_Tilde)\P)-H33+PhKerr;
end
```

With the knowledge of the receptance matrix at the connection point $[H_{44}]$ and the transfer matrix obtained from the FEA of the standalone tool, the connection is made using the following script based on Eq. (7).

```
%%    add tool
for frq_idx=2:size(frqM,1)
      for k=1:5
          for l=1:5
              H_11(k,l)=H_tool{1,1,k,l}(frq_idx);
              H_13(k,l)=H_tool{1,3,k,l}(frq_idx);
              H_31(k,l)=H_tool{3,1,k,l}(frq_idx);
              H_33(k,l)=H_tool{3,3,k,l}(frq_idx);
          end
      end
      G_11Tool{frq_idx}=H_11-H_13*((H_33+H44{frq_idx})\H_31);
end
```

G_11Tool is the sought FRF at the end of the tool, which is stored in a cell structure. This method of storage, unlike a multidimensional array, allows for matrix operations with the obtained FRF matrix.

Funding The results were achieved from funds to support the development of Science & Research at the Faculty of Mechanical Engineering of the Czech Technical University in Prague.

Declarations

Competing interests The authors declare no competing interests.

References

1. Schmitz T, Betters E, Budak E, Yuksel E, Park S, Altintas Y (2023) Review and status of tool tip frequency response function prediction using receptance coupling. Precis Eng 79:60–77
2. Schmitz T, Duncan S (2005) Three-component receptance coupling substructure analysis for tool point dynamics prediction. J Manuf Sci Eng 127(4):781–790
3. Kim J-W, Lee J-W, Kim K-W, Kang J-H, Yang M-S, Kim D-Y, Lee S-Y, Jang J-S (2021) Estimation of the frequency response function of the rotational degree of freedom. Appl Sci 11(18):8527
4. Ji Y, Dong H, Yu L, Ren F, Bi Q, Wang Y (2022) Determining rotating tool-tip FRFs by measuring holder-point FRFs based on a robust frequency-based substructure method. Mech Syst Signal Process 164:108228
5. Ji Y, Yu L, Bi Q, Wang Y, Ren F (2020) A robust RCSA-based method for the in-situ measurement of rotating tool-tip FRFs. J Manuf Sci Eng 142(8):081004
6. Ozsahin O, Ritou M, Budak E, Rabréau C, Le Loch S (2019) Identification of spindle dynamics by receptance coupling for non-contact excitation system. Procedia CIRP 82:273–278
7. Kumar U, Schmitz T (2012) Spindle dynamics identification for receptance coupling substructure analysis. Precis Eng 36:435–443
8. Brecher C, Chavan P, Fey M, Daniels M (2016) A modal parameter approach for receptance coupling of tools. MM Sci J 1032–1034
9. Schmitz T, Honeycutt A, Gomez M, Stokes M, Betters E (2019) Multi-point coupling for tool point receptance prediction. J Manuf Process 43:2–11
10. D`Ambrogio W, Fregolent A (2016) Substructure decoupling without using rotational DoFs: fact or fiction? Mech Syst Signal Process 72–73:499–512
11. Mancisidor I, Urkiola A, Barcena R, Munoa J, Dombovari Z, Zatarain M (2014) Receptance coupling for tool point dynamic prediction by fixed boundaries approach. Int J Mach Tools Manuf 78:18–29
12. Park S, Altintas Y, Movahhedy M (2003) Receptance coupling for end mills. Int J Mach Tools Manuf 43:889–896
13. Montevecchi F, Grossi N, Scippa A, Campatelli G (2017) Two-poins-based receptance coupling method for tool-tip dynamics prediction. Mach Sci Technol 21:136–156
14. Liao J, Yu D, Zhang J, Feng P, Wu Z (2018) An efficient experimental approach to identify tool point FRF by improved receptance coupling technique. Int J Adv Manuf Technol 94:1451–1460
15. Ji Y, Bi Q, Zhang S, Wang Y (2018) A new receptance coupling substructure analysis methodology to predict tool tip dynamics. Int J Mach Tools Manuf 126:18–26
16. Qi B, Sun Y, Li Z (2017) Tool point frequency response function prediction using RCSA based on Timoshenko beam model. Int J Adv Manuf Technol 92:2787–2799
17. Albertelli P, Goletti M, Monno M (2013) An improved receptance coupling substructure analysis to predict chatter free high speed cutting conditions. Procedia CIRP 12:19–24
18. Gibbons TJ, Ozturk E, Sims ND (2017) Rotational degree-of-freedom synthesis: an optimised finite difference method for non-exact data. J Sound Vib 412:207–221
19. Gibbons TJ, Ozturk E, Xu L, Sims ND (2020) Chatter avoidance via structural modification of tool-holder geometry. Int J Mach Tool Manuf 150:103514
20. Karatas G, Ozsahin O, Ozguven HN, Budak E (2021) Design optimization of tool holder extension for enhanced chatter stability by using component mode tuning method. Procedia CIRP 101:294–297
21. Mohammadi Y, Azvar M, Budak E (2018) Suppressing vibration modes of spindle-holder-tool assembly through FRF modification for enhanced chatter stability. CIRP Ann Manuf Technol 67:397–400
22. Munoa J, Beudaert X, Dombovari Z, Altintas Y, Budak E, Brecher C, Stepan G (2016) Chatter suppression techniques in metal cutting. CIRP Ann Manuf Technol 65(2):785–808
23. Postel M, Ozsahin O, Altintas Y (2018) High speed tooltip FRF predictions of arbitrary tool-holder combinations based on operational spindle identification. Int J Mach Tools Manuf 129:48–60
24. Kiran K, Satyanarayana H, Schmitz T (2017) Compensation of frequency response function measurements by inverse RCSA. Int J Mach Tools Manuf 121:96–100
25. Ozsahin O, Ozguven HN, Budak E (2010) Analysis and compensation of mass loading effect of accelerometers on tool point FRF measurement for chatter stability predictions. Int J Mach Tools Manuf 50:585–589
26. Tunc LT (2018) Prediction of tool tip dynamics for generalized milling cutters using the 3D model of the tool body. Int J Adv Manuf Technol 95:1891–1909
27. Brecher C, Chavan P, Fey M (2021) Efficient joint identification and fluted segment mdelling of shrink-fit tool assemblies by updating extended tool models. Prod Eng Res Devel 1(15):21–33
28. Klerk D, Rixen D, Voormeeren S (2008) General framework for dynamic substructuring: history, review, and classification of techniques. AIAA J 46(5):1169–1181
29. Y. Ji, Y. Yu, Q. Bi and H. Zhao, (2023) "Calibration rod selection strategy in RCSA-based method for reliable calculation of milling tool-tip FRFs in rotating conditions," .Int J Mach Tool Manuf 187 104016
30. Mostaghimi H, Park SS, Lee DY, Nam S, Nam E (2023) Prediction of tool tip dynamics through machine learning and inverse receptance coupling. Int J Precis Eng Manuf 24(10):1739–1752